JACC: BASIC TO TRANSLATIONAL SCIENCE VOL. 5, NO. 4, 2020

CLINICAL RESEARCH

In Situ Immune Profiling of Heart Transplant Biopsies Improves Diagnostic Accuracy and Rejection Risk Stratification

Eliot G. Peyster, MD,[a] Chichung Wang, MS,[b] Felicia Ishola, BS,[b] Bethany Remeniuk, PhD,[b] Clifford Hoyt, MS,[b] Michael D. Feldman, MD, PhD,[c] Kenneth B. Margulies, MD[a]

VISUAL ABSTRACT

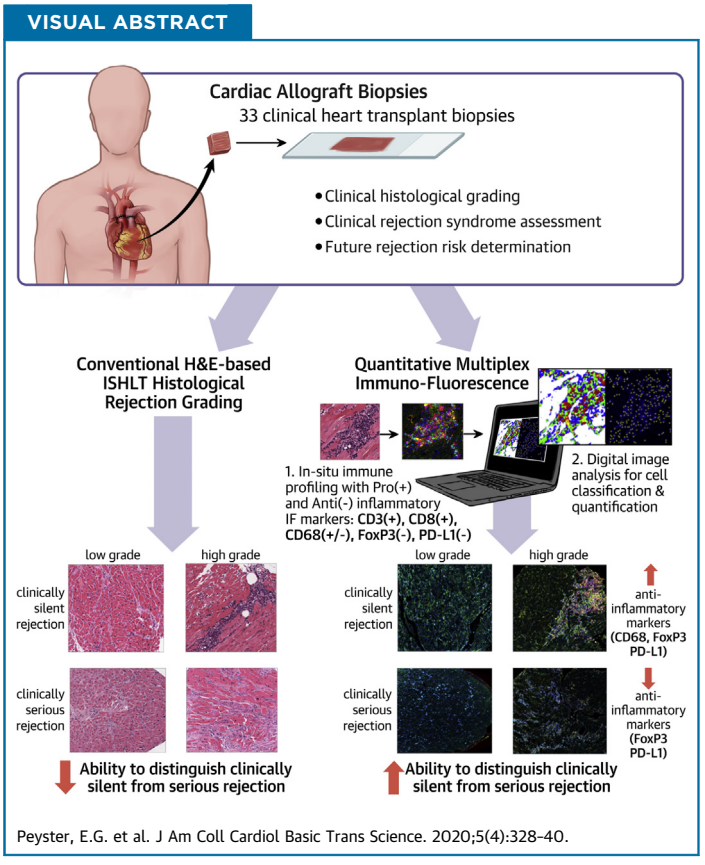

Peyster, E.G. et al. J Am Coll Cardiol Basic Trans Science. 2020;5(4):328-40.

HIGHLIGHTS

- **Quantitative multiplexed immune-phenotyping of cardiac allograft biopsies provides novel diagnostic and prognostic information about allograft health.**
- **Reduced proportions of cells expressing PD-L1 and FoxP3 are associated with clinical evidence of serious allograft injury, even when conventional histologic analysis provides falsely reassuring histologic rejection grades.**
- **The proportions of PD-L1- and FoxP3-expressing cells are dynamic within cardiac allografts, and reduced levels can precede future rejection.**

ISSN 2452-302X https://doi.org/10.1016/j.jacbts.2020.01.015

SUMMARY

Recognizing that guideline-directed histologic grading of endomyocardial biopsy tissue samples for rejection surveillance has limited diagnostic accuracy, quantitative, in situ characterization was performed of several important immune cell types in a retrospective cohort of clinical endomyocardial tissue samples. Differences between cases were identified and were grouped by histologic grade versus clinical rejection trajectory, with significantly increased programmed death ligand 1+, forkhead box P3+, and cluster of differentiation 68+ cells suppressed in clinically evident rejections, especially cases with marked clinical-histologic discordance. Programmed death ligand 1+, forkhead box P3+, and cluster of differentiation 68+ cell proportions are also significantly higher in "never-rejection" when compared with "future-rejection." These findings suggest that in situ immune modulators regulate the severity of cardiac allograft rejection. (J Am Coll Cardiol Basic Trans Science 2020;5:328–40)

ABBREVIATIONS AND ACRONYMS

CAR = cardiac allograft rejection

CD = cluster of differentiation

EMB = endomyocardial biopsy

FoxP3 = forkhead box P3

H-score = histology score

IF = immunofluorescence

ISHLT = International Society of Heart and Lung Transplantation

PD-L1 = programmed death ligand 1

QmIF = quantitative multiplex immunofluorescence

Cardiac allograft rejection (CAR) is a serious concern among transplant recipients, occurring in roughly one-third of patients in the first year post-transplantation and conferring an increased risk of short- and long-term graft failure. Because of the high morbidity and mortality associated with CAR, the International Society for Heart and Lung Transplantation (ISHLT) has recommended regular surveillance endomyocardial biopsy (EMB) with standardized histologic grading for CAR since 1990.

Unfortunately, the guideline-recommended ISHLT grading scheme suffers from a lack of prognostic accuracy, correlating poorly with the clinical trajectory of a current rejection event and lacking the ability to stratify patients by future CAR risk (1–4). A failure of histologic grade to correlate with a patient's imminent clinical trajectory can cause false reassurance in some cases and false alarm in others, with resultant treatment delays or overtreatment posing serious risks to patients. Because conventional ISHLT histologic grade never provides longer-term risk stratification, surveillance testing and immunosuppression-weaning protocols cannot be tailored to individual CAR risk. As a result, low-risk patients undergo more EMB procedures and more aggressive immunosuppression than are needed with attendant risks of infection and procedural complications. On the other hand, high-risk patients undergo premature weaning of immunosuppression, resulting in potentially avoidable rejection episodes. Both of these scenarios represent opportunities for better outcomes through improved diagnostic accuracy and greater prognostic insight.

The traditional approach to morphologic CAR detection involves the identification and rough quantification of basophilic immune cells on hematoxylin and eosin-stained slides. This approach provides few insights into the specific types (and therefore, functions) of the immune cells present within EMB tissue. Expert panels have explicitly acknowledged the need for "further characterization of the nature of the

From the [a]Cardiovascular Research Institute, University of Pennsylvania, Philadelphia, Pennsylvania; [b]Akoya Biosciences, Hopkinton, Massachusetts; and the [c]Department of Pathology and Laboratory Medicine, University of Pennsylvania, Philadelphia, Pennsylvania. Research reported in this publication was supported by the Gund Family Fund at the University of Pennsylvania and the National Center for Advancing Translational Sciences of the National Institutes of Health under award number TL1TR001880. The content is solely the responsibility of the authors and does not necessarily represent the official views of the National Institutes of Health. Mr. Wang, Ms. Ishola, and Ms. Remeniuk are employed by Akoya Biosciences. Mr. Hoyt is employed by Akoya Biosciences; and owns Akoya Biosciences stock and stock options. Dr. Feldman is an equity holder and has technology licensed to both Elucid Bioimaging and Inspirata Inc.; has served as a scientific advisory consultant for Inspirata Inc.; served on the scientific Advisory Board of Inspirata Inc.; and has consulted for Phillips Healthcare, XFIN, and Virbio. Dr. Margulies has received research grants from Thoratec Corporation, Merck, Sanofi-Aventis USA, and GlaxoSmithKline; has served as a scientific consultant for American Regent; and has served as an Advisory Board member for Pfizer and MyoKardia. Dr. Peyster has reported that he has no relationships relevant to the contents of this paper to disclose.

The authors attest they are in compliance with human studies committees and animal welfare regulations of the authors' institutions and Food and Drug Administration guidelines, including patient consent where appropriate. For more information, visit the *JACC: Basic to Translational Science* author instructions page.

Manuscript received December 15, 2019; revised manuscript received January 24, 2020, accepted January 24, 2020.

inflammatory infiltrate" to extract additional clinically relevant information from EMB samples (5). Despite this 15-year-old call to action, there has been very limited application of tissue-level immune phenotyping in human heart transplant tissues. This stands in contrast to oncologic and rheumatologic medicine, where deeper phenotyping of immune populations and immune effector pathways have resulted in improved risk stratification and better targeting of therapeutic strategies (6–12).

In this paper, we report novel proof-of-concept studies applying a state-of-the-art, fully quantitative, multiplex immunofluorescence (QmIF) methodology on archived clinical EMB tissue samples, with a focus on uncovering immune phenotypes that can improve the diagnostic and prognostic performance of histologic analysis for CAR. Using a custom panel of IF markers focused on cell-mediated immune responses and modified from commercially available panels validated in multiple oncologic publications (13–17), we performed in situ identification and quantification of cluster of differentiation 3 (CD3), CD8, CD68, forkhead box P3 (FoxP3), and programmed death ligand 1 (PD-L1). Due to limited research in human heart transplant tissues, the rationale for the markers selected for this cell-mediated rejection panel comes predominantly from animal models and renal transplantation (18–33). T cells are implicated in most cases of CAR, but are in actuality a heterogeneous group of cells capable of exerting pro-inflammatory and anti-inflammatory effects under different conditions. As a result, quantification of the pan-T-cell marker CD3 in addition to markers of T-cell subtypes and effectors was the objective of this proof-of-concept work. Within this context, our novel application of QmIF demonstrated striking new diagnostic and prognostic insights beyond the standard ISHLT grade, supporting potential benefits from further application and refinement of the immune-phenotyping panel.

METHODS

COHORT CONSIDERATIONS. The study cohort was selected from the transplant records at the Hospital of the University of Pennsylvania and consisted of biopsy events that occurred between 2007 and 2013. Cases were manually selected to allow for exploration of the potential diagnostic and prognostic implications of performing immune phenotyping within EMB tissue. Specifically, the cohort of 46 transplant EMB described in this paper was selected to permit assessments of how immune cell populations differ between tissues with low versus high ISHLT grades, between tissues corresponding to clinically silent versus clinically evident rejection trajectories, and between tissues from patients who will go on to experience serious rejection (future rejection) versus those who will not (never rejection). The retrospective chart review and analysis of archived tissue specimens employed in this research were approved by the Institutional Review Board at the University of Pennsylvania.

For these retrospective cases, the ISHLT histologic grade assigned by the attending pathologist at the time of the EMB procedure was used as the reference standard for rejection diagnosis. These grades were further simplified by assigning a binary histologic grade label: "low-grade" rejection was defined as ISHLT 2004 consensus criteria histologic grades 0R or 1R and "high-grade" rejection was defined as ISHLT histologic grade 2R or 3R. This grouping typically defines the distinction used to determine whether augmented immunosuppressive therapy is prescribed (34).

For the same 46 EMB events, the distinction between "clinically silent" and "clinically evident" rejection was made based on a set of major and minor criteria to determine whether allograft injury was present. Clinical metadata from within 7 days of each EMB event were collected to allow for determination of clinical trajectory. These data were derived from electronic health record-documented symptoms, physical exam findings, lab results, echocardiographic parameters, electrocardiogram findings, and invasive hemodynamic data. The major criteria in **Table 1** for differentiating clinically evident from clinically silent rejection trajectories are based on definitions of "hemodynamic compromise" in previous prospective investigations of allograft rejection (35–37) and provide high specificity for clinically significant rejection. The minor criteria in **Table 1** permit identification of clinically significant cases with greater sensitivity. By design, a subset of each clinical trajectory category represented an EMB with clinical-histologic discordance (low-histologic grade meeting criteria for clinically evident rejection, or high-histologic grade with none of the criteria met for clinically evident rejection). All determinations of clinically evident versus clinically silent rejection were completed prior to the performance of immunostaining.

Finally, the 19 EMB in this cohort that were categorized as low ISHLT grade and clinically silent were further classified by the patient-level incidence of future serious CAR events. These EMB were assigned a binary label as either "future rejection" or "never rejection," based on whether a serious CAR event occurred within the first 3 years post-transplantation. These cases allow for assessment of whether

TABLE 1 Criteria for Determining Clinically Evident Rejection

Admission to hospital for rejection treatment, along with 1 major or 2 minor criteria:
Major criteria
Cardiac index ≤2.0 and use of inotropes
Absolute decrease in LVEF of ≥20%
Minor criteria
Cardiac index ≤2.3, provided this represents a ≥20% decrease in cardiac index from baseline
Right atrial pressure >10 mm Hg or pulmonary capillary wedge pressure >18 mm Hg provided this represents a ≥40% increase from baseline
Absolute decrease in LVEF of ≥10% and to a level of ≤50%
New arrhythmia—atrial fibrillation, flutter, or ventricular arrhythmia
New low voltage ECG not due to pericardial effusion or pulmonary disease
Cardiac troponin elevated ≥3× the upper limit of normal and ≥3× the patient's baseline, not due to coronary artery disease/graft vasculopathy
Documented diagnosis of increased LV wall thickness and an LV wall thickness increase of >2 mm from baseline value
Documented new or worsened right ventricular dysfunction by echo
Documented clinical signs or symptoms of rejection or heart failure: Signs = new gallop, new low pulse volumes, new rales. Symptoms = new or worsened dyspnea, orthopnea, exercise intolerance documented by provider as likely due to cardiac cause.

ECG = electrocardiogram; LV = left ventricular; LVEF = left ventricular ejection fraction.

meaningful differences occur in IF markers in advance of a serious CAR event.

RETROSPECTIVE SAMPLE ACQUISITION AND PREPARATION. All EMB tissues analyzed for this study had been sampled using a standard percutaneous method, fixed in 4% paraformaldehyde, and embedded in paraffin wax as per usual post-transplantation clinical care and pathology laboratory workflows at the Hospital of the University of Pennsylvania. Five, 4-μm thick serial sections were cut from formalin-fixed paraffin-embedded blocks and mounted onto positively charged glass microscope slides (48382-119; VWR Corp., Radnor, Pennsylvania) used for immunohistochemistry, with 1 section per slide. All cut, unstained tissue sections were stored in a nitrogen chamber to minimize oxidation and degradation of tissue epitopes. In addition to EMB slides, 2 slides from native (nontransplant) heart tissue obtained from cadaveric organ donors and 1 slide from human lymph node tissue were used as "negative" and "positive" staining controls, respectively.

TARGET SELECTION FOR MULTIPLEX IMMUNOFLUORESCENCE. The cytotoxic T-cell marker CD8 was selected due to recognition that this cell population is a primary effector of myocyte injury during cellular rejection (18–20). Regulatory T-cell transcription factor FoxP3 was selected due to the immune-modulatory, anti-inflammatory effects these interleukin-10 and transforming growth factor-βsecreting cells are thought to exert in renal allografts (21–23) and animal models of heart transplantation (24,25). The monocyte lineage marker CD68 is used in the diagnosis of antibody-mediated rejection, but it has also been implicated in cellular rejection, albeit with conflicting results on the effects these cells exert (26,27). Finally, PD-L1 is 1 component of the PD-L1/PD1 immune "checkpoint" molecules that interact to suppress cytotoxic actions of activated T cells. Though checkpoint inhibitors used in cancer immunotherapy have been implicated in myocarditis, a role for checkpoint molecules in human heart transplantation has included only case reports of severe rejection following oncologic PD1/PD-L1 inhibitor treatment (28–30). However, the checkpoint pathway has been recognized for its role in abrogating T-cell responses and promoting tolerance in animal models of organ transplantation (31–33).

QUANTITATIVE MULTIPLEX IMMUNOFLUORESCENCE METHODS. All study tissue samples were assigned deidentified study identifications and sent to Akoya Biosciences (Hopkinton, Massachusetts) for multiplex staining, slide digitization, and per-slide image quantification. The scientific team performing staining and image quantification was blinded to patient outcomes. Details of deparaffinization, reagent preparation, and automated staining workflows are described in the Supplemental Appendix. Details on antibodies utilized for multiplex staining are summarized in Supplemental Table 1.

Whole slide multispectral image acquisition. High-throughput whole slide multispectral (MOTiF) image scans were acquired on the Vectra Polaris (Akoya Biosciences) at 20× using narrow, multiband filters. Exposure times were set to avoid saturation.

Image quality control and annotation selection. Following image acquisition, scans were imported into Phenochart (Akoya Biosciences) to assess the image quality. Up to 5 1 × 1 regions of interest were

FIGURE 1 Flow Diagram of Study Cohort, With Subgroups

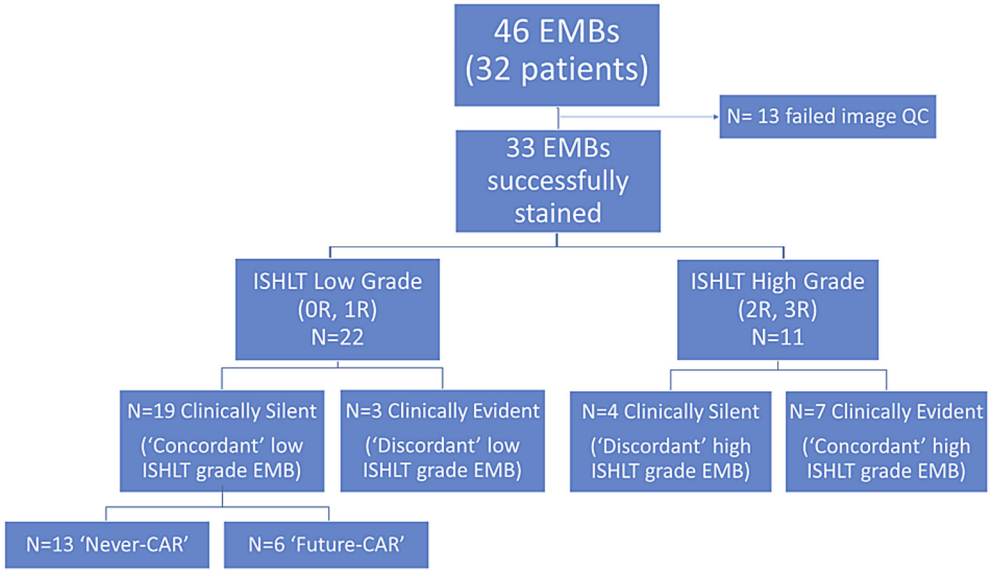

The flow diagram depicts the study cohort with subgroups. CAR = cardiac allograft rejection; EMB = endomyocardial biopsy; ISHLT = International Society for Heart and Lung Transplantation; QC = quality control.

annotated for each sample to conduct quantitative image analysis. Some samples were unable to yield 5 regions of interest due to confounding factors, such as tissue folds, small tissue biopsy size, or large areas without myocardium (e.g., vessels, fibrosis, fat).

Quantitative multispectral image analysis. A spectral library was created from the stained library slides, and the autofluorescence spectrum was isolated using the autofluorescence slide. All annotated regions of interest were imported into a new project in inForm Tissue Finder (Akoya Biosciences) and were spectrally unmixed using the generated spectral library. Of note, the image analyst was blinded to the slide cohort categories to avoid bias.

Staining quality control. Individual fluorophore signal intensities, in normalized counts, were assessed on the multiplex imagery following spectral unmixing to confirm proper staining intensity levels and absence of residual cross talk.

InForm analysis workflow. The Trainable Tissue Segmentation module was used to automatically segment all samples into total cardiac tissue and background based on hand-drawn training regions. Cell segmentation was conducted using the Adaptive Cell Segmentation, which uses algorithms to account for variations in staining and background levels within and across images to identify cellular compartments from multiple image planes. The algorithm first identifies the cell nuclei (via 4′,6-diamidino-2-phenylindole staining), followed by the cell membrane and cytoplasm for each, and has further settings for cell splitting and staining quality. The Phenotyping module, which utilizes a user-trainable random forest classifier, learned and phenotyped all markers, except for PD-L1, in which the staining intensity was scored per cell on a 0 to 3+ scale using thresholding to enable histology score (H-score) calculations. All cell segmentation and scoring data and imagery were exported for further analysis.

STATISTICAL METHODS. Raw cell count (and PD-L1 intensity) data generated by inForm quantitative image analysis were sent to the University of Pennsylvania for further analysis. Cases were analyzed by pre-specified groups as described in "cohort considerations." For CD3+, CD8+, CD68+, and PD-L1 cell count data, values were normalized by total cell counts to account for differences in tissue size and myocardial area. $FoxP3^+$ cells were normalized by the total T-cell (CD3+) cell count. Groupwise chi-squared testing was performed on the normalized cell count data. Comparisons included cases grouped by high versus low ISHLT histologic grade, by clinically evident versus clinically silent rejection determination, and by patient-level future-rejection versus never-rejection label. Cases were also analyzed by

contingency table designation, as it pertains to the concordance between high/low ISHLT grade and the presence or absence of clinically evident allograft injury (e.g., "concordant positive" = high ISHLT grade/clinically evident CAR, "concordant negative" = low ISHLT grade/clinically silent CAR, "discordant positive" = high ISHLT grade/clinically silent CAR, and "discordant negative" = low ISHLT grade/clinically evident CAR).

Semiquantitative analysis of PD-L1 staining intensity was also performed, with PD-L1+ status placed into 1 of 4 categories based on intensity (level 0 = no PD-L1, level 1 = low intensity, level 2 = moderate intensity, level 3 = high intensity). PD-L1 H-scores were based on a method described previously (38). Briefly, the total number of cells and the percentage of cells in each PD-L1-staining level were counted in 3 randomly selected fields under high magnification. PD-L1 H-score was then calculated for each case according to the following formula: H-score = 0 × % of level-0 cells + 1 × % of level-1 intensity cells + 2 × % of level-2 intensity cells + 3 × % of level-3 intensity cells. Because H-scores were tabulated on a per-patient basis rather than a per-cell basis, a per-patient analysis of this metric was performed using a Wilcox rank-sum test to assess differences between pre-specified study groups.

All statistical analysis was performed in Stata version 15, (StataCorp, College Station, Texas), and p values <0.05 were considered significant for all analyses.

RESULTS

A total of 46 EMB episodes plus 3 additional control tissues were selected for this analysis, and their characteristics are detailed in Supplemental Table 2. In total, 36 of 49 (74%) of the formalin-fixed paraffin-embedded tissue slides (including the 3 non-EMB control samples) submitted for QmIF underwent successful staining, quality control assessment, and comprehensive quantitative analysis. Of the 33 transplantation EMB cases that completed study staining and analysis (see **Figure 1**), 22 had low ISHLT grades (1R and 0R) and 11 had high ISHLT grades (2R and 3R). Of the cases with low ISHLT grades, 19 had clinically silent rejection and 3 had clinically evident rejection. Of the cases with high ISHLT grades, 7 had clinically evident rejection and 4 had clinically silent rejection. None of the instances of clinically evident rejections corresponding to low ISHLT grades met ISHLT criteria for antibody-mediated rejection (39). Specifically, none had new donor-specific antibodies or significant C4d deposition by clinical IF staining. Of the 19 cases with low ISHLT grades and clinically silent rejection, 6 would go on to have a future rejection within ~1 year and 13 would never reject over the next 3 years. Of the 4 discordant high ISHLT grade EMB associated with a clinically silent course, none manifested evidence of clinically evident allograft rejection in the subsequent 3 months.

TISSUE IMMUNOPHENOTYPING RESULTS. For the 33 EMB cases that completed QmIF staining, there were a total of 191,331 cells in the regions that underwent quantitative analysis, with CD3+ cells representing the most common immune cell type, as summarized in **Table 2**.

Table 3 shows the study results grouped by ISHLT grade (high vs. low) and by clinical rejection syndrome (clinically silent vs. clinically evident). High-grade EMB have significantly higher proportions of CD3+ and CD8+ cells than do low-grade EMB ($p < 0.001$). Grade-agnostic grouping by rejection syndrome severity demonstrates analogous results, with serious, clinically evident rejection events having higher proportions of CD3+ and CD8+ cells than clinically silent rejection events ($p < 0.001$). **Figure 2A** provides a compelling visual demonstration of how these conventional T-cell markers correlate predominantly with grade classification and provide little help for discriminating between cases with versus without serious clinical rejection syndromes.

High-grade EMB also have significantly higher proportions of macrophage marker CD68 when compared with low-grade EMB ($p < 0.001$), but unlike the traditional T-cell markers CD3 and CD8, the opposite relationship is seen when cases are grouped by the severity of the clinical rejection syndrome. Clinically silent rejection events have a significantly higher proportion of CD68+ cells than do clinically evident rejection events ($p < 0.001$). An examination of the results from EMB with clinical-histologic discordance provides the explanation for these opposing results (**Table 4, Figure 2B**), with discordant high-grade cases manifesting by far the highest proportion of CD68+ cells (5.45%; $p < 0.001$) whereas discordant low-grade cases manifest the lowest (0.14%; $p < 0.001$).

Cells expressing the regulatory T-cell marker FoxP3 are twice as abundant in clinically silent rejection events, as compared with clinically evident rejection both within the low-histologic grade and the high-histologic grade cohort ($p < 0.001$ for both). Even more striking, PD-L1+ cells were more than 4-fold more abundant in clinically silent cases compared with clinically evident cases, regardless of ISHLT grade. **Table 4 and Figure 2B** highlight the strong, grade-independent correlation of FoxP3 and

TABLE 2 QmIF Total Cell Count Results

Cell Type	Cell Count	% of Total
CD8+	8,646	4.52
CD3+	15,571	8.14
CD68+	2,814	1.47
FoxP3+	382	0.20
PDL1+	8,932	4.67
DAPI (total cells)	191,331	100.00

CD3+ = cluster of differentiation 3+; DAPI = 4′,6-diamidino-2-phenylindole; FoxP3+ = forkhead box P3+; PD-L1+ = programmed death ligand 1; QmIF = quantitative multiplex immunofluorescence.

PD-L1, with similarly high proportions found either in low- or high-grade clinically silent EMB and similarly low proportions found in either low- or high-grade clinically evident EMB.

The per-patient PD-L1 H-score, a composite measure incorporating both PD-L1 staining prevalence and signal intensity, is strongly associated with clinical rejection syndrome but not with histologic grade (Tables 3 and 4, Figure 3B). Patients with clinically silent rejection syndromes, whether the EMB received a high or low grade, manifest PD-L1 H-scores that are at least 4× higher than those seen for clinically evident rejection events of either grade class. Illustrative hematoxylin and eosin- and QmIF-stained digital slides for high and low ISHLT grades with both concordant and discordant clinical rejection syndromes are shown in Figure 3.

Immunophenotyping future- and never-rejection cases. To assess whether immune phenotypes differ between patients who will suffer important rejection events in the future and those who will not, we analyzed the subset of cases in which serial, concordant, low-grade EMB were available for individual patients. These patients were assigned a binary label as either future rejection or never rejection. For the pre-specified future-rejection subgroup, 6 EMB preceding a high-grade, clinically evident rejection event successfully completed the QmIF analysis. This included 3 EMB obtained >6 months prior to a rejection and 3 EMB obtained 3 to 6 weeks prior to a rejection. For the never-rejection group, there were 13 EMB, but in only 1 instance was the same patient sampled twice (due to a high, and likely by chance, rate of staining/image quality issues with the serial never-rejection subgroup). From the 6 future-rejection EMB samples, a total of 26,371 cells were analyzed, whereas the 13 EMB from the never-rejection samples provided 48,245 cells for analysis.

Despite relatively few cases, every QmIF marker except CD68 displayed statistically significant differences between future-rejection cases and never-rejection cases, as shown in Table 5. Though these analyses were performed on biopsies that were uniformly of low-histologic grade at a time when there was no evidence of allograft dysfunction or injury, the future-rejection group more closely resembles the clinically evident and high-grade rejection groups than it does the clinically silent or low-grade groups. When the future-rejection group is analyzed by temporal proximity to the incident severe rejection event, an apparent progression emerges: compared with never-rejection cases, future-rejection cases at >6 months prior to rejection have a moderately reduced proportion of FoxP3+ and PD-L1+ cells. By 3 to 6 weeks before clinically evident rejection, there is a dramatic and statistically significant drop-off to extremely low levels for FoxP3+, CD68+, and the PD-L1+ cells (Table 5, Figure 4).

DISCUSSION

These proof-of-concept studies applying QmIF technology within the cardiac transplantation population provide compelling evidence for the feasibility and utility of immune phenotyping to improve the diagnostic and prognostic value of allograft EMB specimens. First, using archived formalin-fixed, paraffin-embedded tissue blocks—some more than 10

TABLE 3 QmIF Results by Immune Cell Type With Cases Grouped by Clinical Rejection Trajectory and Conventional Histologic Grade

Marker	Low Grade	High Grade	p Value	Clinically Silent	Clinically Evident	p Value
CD8+	1.16 ± 0.04 (1,049/90,731)	7.55 ± 0.08 (7,597/100,600)	<0.001	2.93 ± 0.05 (2,754/94,098)	6.06 ± 0.07 (5,892/97,233)	<0.001
CD3+	3.3 ± 0.06 (2,995/90,731)	12.5 ± 0.1 (12,576/100,600)	<0.001	5.6 ± 0.07 (5,266/94,098)	10.6 ± 0.09 (10,305/97,233)	<0.001
CD68+	0.83 ± 0.03 (757/90,731)	2.04 ± 0.04 (2,057/100,600)	<0.001	1.91 ± 0.04 (1,797/94,098)	1.05 ± 0.03 (1,017/97,233)	<0.001
FoxP3+*	3.21 ± 0.32 (96/2,995)	2.27 ± 0.13 (286/12,576)	0.039	3.61 ± 0.26 (190/5,266)	1.86 ± 0.13 (192/10,305)	<0.001
PD-L1+	6.48 ± 0.08 (5,876/90,731)	3.04 ± 0.05 (3,056/100,600)	<0.001	7.86 ± 0.09 (7,392/94,098)	1.58 ± 0.04 (1,540/97,233)	<0.001
PD-L1 H-score per EMB	3 (1–16)	4 (1–11)	0.88	5 (2–16)	1 (0–2)	0.018

Values are percentage of total cells ± SE (n/N) or median (interquartile range). *Percentage of CD3+ cells ± SE.
EMB = endomyocardial biopsy; H-score = histology score; other abbreviations as Table 1.

FIGURE 2 **QmIF Results Grouped by ISHLT Grade and Clinical Status**

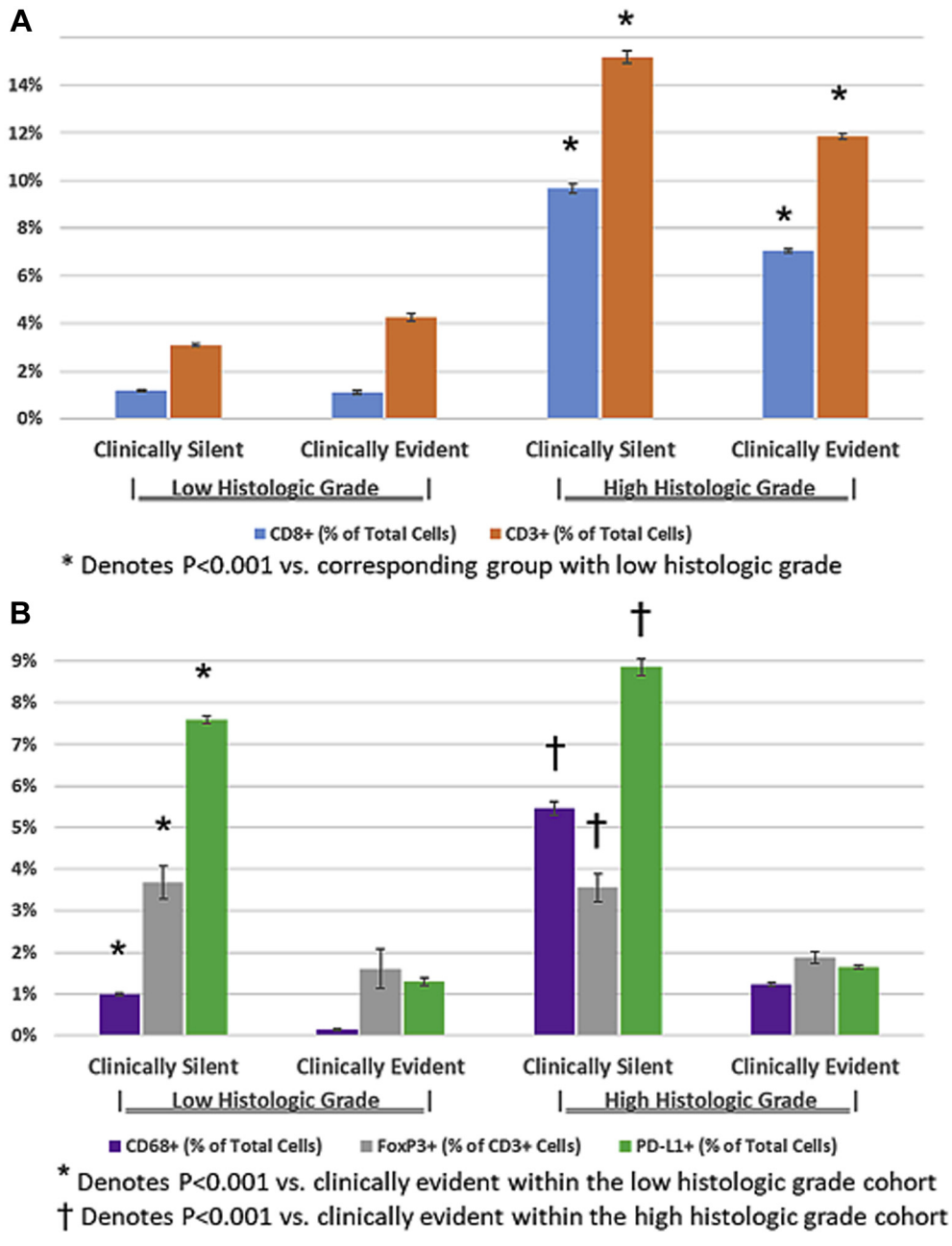

(A) Quantitative multiplex immunofluorescence (QmIF) results for cluster of differentiation 3+ (CD3+) and CD8+ cells, grouped by ISHLT grade and subgrouped based on concordance or discordance between ISHLT grade and clinical evidence of rejection (see Table 1). Proportions of CD3+ and CD8+ cells correlate well with ISHLT grade and Do not help discriminate between cases classified by clinical rejection trajectory. **(B)** QmIF results for CD68+, forkhead box P3+ (FoxP3+), and programmed death ligand 1+ (PD-L1+) cells, grouped by ISHLT grade and subgrouped based on concordance or discordance between ISHLT grade and clinical evidence of rejection (Table 1). Within low ISHLT grades, there are significant differences between cases with clinically silent versus evident rejection (CD68+: 0.99% vs. 0.14%; $p < 0.001$; FoxP3+: 3.68% vs.1.60%; $p < 0.001$; PD-L1+: 7.59 vs. 1.3; $p < 0.001$). Within the high ISHLT grades, there are also significant differences between silent and evident rejection (CD68+: 5.45% vs. 1.23%; $p < 0.001$; FoxP3+: 3.55% vs. 1.88%; $p < 0.001$; PD-L1+: 8.85 vs. 1.64; $p < 0.001$). Overall, these QmIF markers correlate much better with clinical rejection severity then they do with traditional ISHLT grade and may provide additional diagnostic value for assessing rejection on EMB. **Error bars** = SE. $p < 0.001$ versus clinically evident within the *low histologic grade cohort and †high histologic grade cohort. Abbreviations as in Figure 1.

TABLE 4 QmIF Results by Immune Cell Type, With Cases Grouped by Contingency Table Designation Based on Concordance Versus Discordance of Clinical Rejection Severity and ISHLT Histologic Grade

	Contingency Table Groups				p Values for Intergroup Comparisons					
Marker	C-Low	D-High	D-Low	C-High	C-Low vs. D-Low	C-Low vs. C-High	C-Low vs. D-High	D-Low vs. C-High	D-Low vs. D-High	D-High vs. C-High
CD8+	1.17 ± 0.04 (871/74,616)	9.67 ± 0.09 (1,883/19,482)	1.1 ± 0.03 (178/16,115)	7.04 ± 0.08 (5,714/81,118)	0.5	<0.001	<0.001	<0.001	<0.001	<0.001
CD3+	3.09 ± 0.06 (2,309/74,616)	15.18 ± 0.11 (2,957/19,482)	4.26 ± 0.07 (686/16,115)	11.86 ± 0.1 (9,619/81,118)	<0.001	<0.001	<0.001	<0.001	<0.001	<0.001
CD68+	0.99 ± 003 (735/74,616)	5.45 ± 0.07 (1,062/19,482)	0.14 ± 0.01 (22/16,115)	1.23 ± 0.03 (995/81,118)	<0.001	<0.001	<0.001	<0.001	<0.001	<0.001
FoxP3+*	3.68 ± 0.39 (85/2,309)	3.55 ± 0.34 (105/2,957)	1.6 ± 0.48 (11/686)	1.88 ± 0.14 (181/9,619)	<0.001	<0.001	0.80	0.60	<0.001	<0.001
PD-L1+	7.59 ± 0.09 (5,667/74,616)	8.85 ± 0.09 (1,725/19,482)	1.3 ± 0.04 (209/16,115)	1.64 ± 0.04 (1,331/81,118)	<0.001	<0.001	<0.001	0.002	<0.001	<0.001
PD-L1 H-score per EMB	4 (2–16)	9 (6–19)	1 (0–2)	1 (0–4)	0.09	0.13	0.24	0.64	0.034	0.037

Values are percentage of total cells ± SE (n/N) or median (interquartile range). *Percentage of CD3+ cells ± SE.
C = concordance; D = discordance; High = high grade; ISHLT = International Society of Heart and Lung Transplantation; Low = low grade; other abbreviations as in Tables 2 and 3.

years old—successful application of Opal multiplex IF staining technology sufficient for advanced quantitative analysis was achieved in the sizable majority of cases. In designing this experiment, we incorporated a "grade-agnostic" framework using the clinically evident and clinically silent labels to classify EMB by the contemporary clinical status of the patient. We hypothesized that QmIF results might suggest mechanisms underlying the frequent discordance between patients' clinical status and the ISHLT grade given to EMB samples. For conventional T-cell markers CD3 and CD8, the QmIF results largely conformed to prior evidence and accepted pathophysiology and do not significantly help discriminate between patients with and without serious rejection syndromes. High ISHLT grades had markedly higher proportions of CD3+ and CD8+ cells, consistent with the higher overall quantity of basophilic lymphocytes seen in standard hematoxylin and eosin slides with high ISHLT histologic grades. Cases grouped by clinical rejection severity followed a similar pattern, with clinically evident rejection having a higher proportion of these T-cell markers. Because ISHLT grading is primarily predicated on rough quantification of lymphocyte foci (within which CD3+ and CD8+ cells predominate), these findings suggest that misgrading is not the primary reason for clinical-histologic disagreement in our discordant case subgroups.

The proportion of CD68+ cells was also significantly higher in high ISHLT grade rejection, consistent with several prior reports in renal transplantation that have suggested that macrophages represent a major (and occasionally predominant) cell line in some cases of cellular rejection (26,27). In contrast, when cases are grouped by clinical status, the proportion of CD68+ cells are significantly lower in EMB associated with more serious, clinically evident rejection syndromes. This finding is driven almost entirely by the cases with clinical-histologic discordance—clinically silent/high-grade EMB have by far the highest proportion of CD68+ cells with a prevalence that is ~40× higher than that seen in clinically evident/low-grade cases (which had by far the lowest proportion). In these clinically silent/high ISHLT grade cases, inspection of the QmIF slide (**Figure 3C4**) reveals robust CD68+ staining within the dense cellular infiltrates, which stands in stark contrast to the modest CD68 staining within the cellular infiltrate of the concordant high ISHLT grade case (**Figure 3D4**). Because discordant high ISHLT grade cases have comparable (or greater) numbers of CD3+ and CD8+ cells, this visual observation makes it tempting to speculate that CD68+ cells may be part of an important "late" protective response, mitigating serious injury to an allograft after lymphocytic infiltration occurs.

The proportion of FoxP3+ cells and cells staining strongly for PD-L1 also differ significantly when cases are grouped by clinical trajectory. Clinically silent rejection events, regardless of ISHLT grade, have significantly higher proportions of both of these anti-inflammatory markers than do clinically evident rejection events. These results raise the possibility that the interactions of immune-modulating cell subtypes and pathways may play a role in determining whether an initial allo-immune response becomes a clinically serious one, though this study was notably not designed to demonstrate such causal relationships. It is worthwhile to highlight that the discordant

FIGURE 3 Representative EMB Cases, With H and E Stained, 7-IF Marker Composite, and Select Single IF Marker Digital Slides

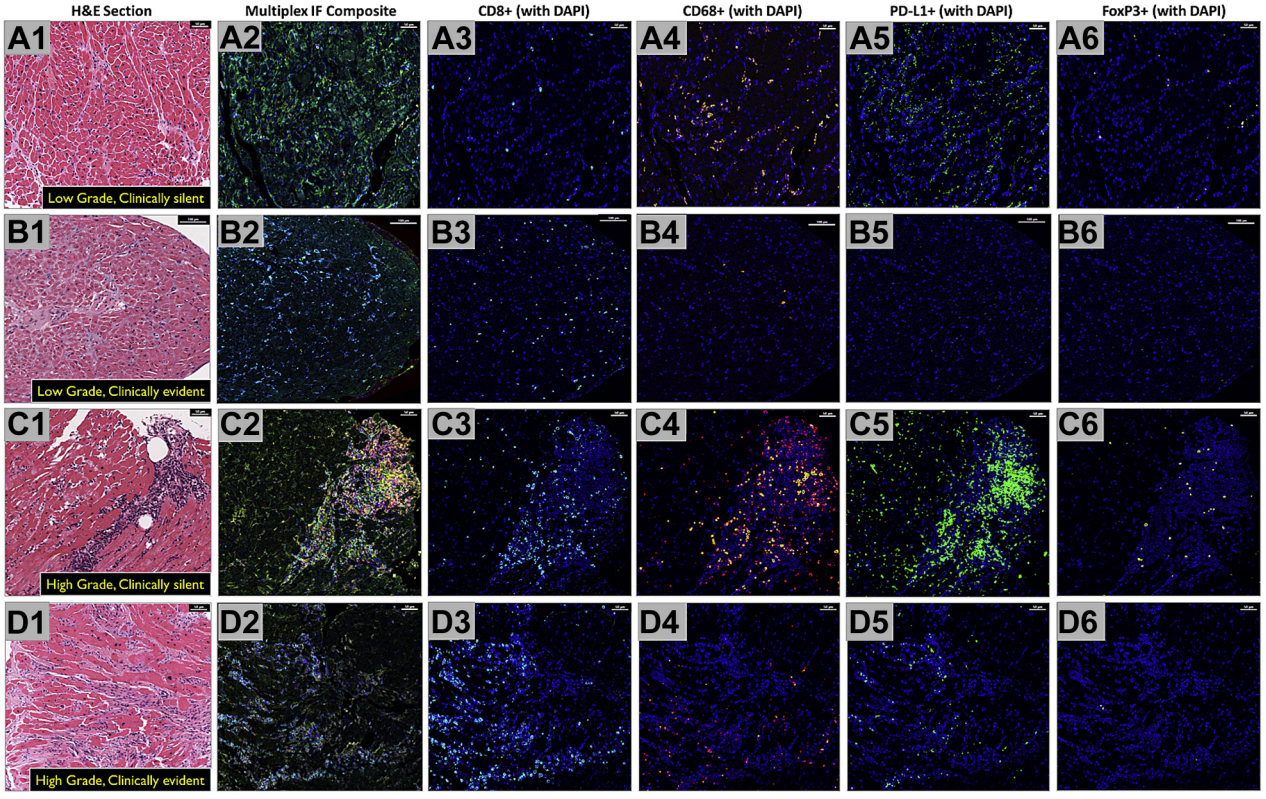

Hematoxylin and eosin (H and E)-stained **(A1, B1, C1, D1),** 7-immunofluorescence (IF) marker multiplex composite **(A2, B2, C2, D2),** and selected single IF marker **(A3 to A6, B3 to B6, C3 to C6, D3 to D6)** EMB slides. **(A)** Images are a representative concordant low ISHLT grade EMB with low ISHLT grade and no clinical evidence of allograft injury. **(B)** Images are from a discordant low ISHLT grade EMB, with low-histologic grade but clinically evident allograft injury. Images are from a discordant high ISHLT grade EMB **(C)** and from a concordant high ISHLT grade EMB **(D).** Although rough estimates of basophilic cellular infiltrates due not appear markedly different within grade in H and E slides (**A1** vs. **B1,** and **C1** vs. **D1**), multiplex IF profiles within grade visibly differ between cases with and without evident allograft injury. Note diffuse PD-L1 **(green)** staining within myocardium of patients with clinically silent CAR **(A5, C5),** in comparison to clinically evident CAR **(B5, D5).** Also note profound PD-L1 and CD68 within cellular infiltrate in discordant high-grade EMB **(C4),** as well as the higher proportion (albeit overall low density) of FoxP3 cells when compared with the concordant high grade EMB (**C6** vs. **D6**). The scale bar is 50 um for **panels in rows A, C, and D**, and 100 um for **panels in row B**. Phrased differently, **panels in rows A, C, and D** are 500 um in total width, while panels in row **B** are 750 um in total width. DAPI = 4′,6-diamidino-2-phenylindole; other abbreviations as in Figures 1 and 2.

cases manifest the most extreme proportions of these potentially allograft-protective markers, with the discordant high-grade cases containing the highest proportions and the discordant low-grade cases containing the lowest. Visual inspection of QmIF slides further highlights the potential importance of PD-L1, with a diffuse PD-L1+ (green) staining pattern seen throughout the myocardium in clinically silent biopsies (Figures 3A5 and 3C5) that is conspicuously absent in clinically evident rejection cases (Figures 3B5 and 3D5). It is also worth highlighting the particularly dense PD-L1 staining seen within the cellular infiltrate of the discordant high ISHLT grade slide (Figure 3C5), which may suggest an active and dynamic PD-L1 presence at the site of an acute immune response.

Overall, the QmIF results of EMB cases grouped by clinical trajectory support the hypothesis that to accurately assess the threat to allograft function,

TABLE 5 QmIF Results for Cases Associated With Future Serious Rejection and Those Who Never Experience Serious Rejection

Marker	Never Rejection	Future Rejection	p Value
CD8+	0.48 ± 0.02 (230/48,245)	2.43 ± 0.05 (641/26,371)	<0.001
CD3+	1.19 ± 0.04 (573/48,245)	6.58 ± 0.08 (1,736/26,371)	<0.001
CD68+	1.01 ± 0.03 (488/48,245)	0.94 ± 0.03 (247/26,371)	0.32
FoxP3+*	10.82 ± 1.30 (62/573)	1.32 ± 0.27 (23/1,736)	<0.001
PD-L1+	10.7 ± 0.1 (5,160/48,245)	1.92 ± 0.04 (507/26,371)	<0.001
PD-L1 H-score per EMB	5 (3-16)	1.5 (0-3)	0.034

Values are percentage of total cells ± SE (n/N) or median (interquartile range). *Percentage of CD3+ cells ± SE. Abbreviations as in Tables 2 and 3.

FIGURE 4 QmIF Results Grouped by Future CAR

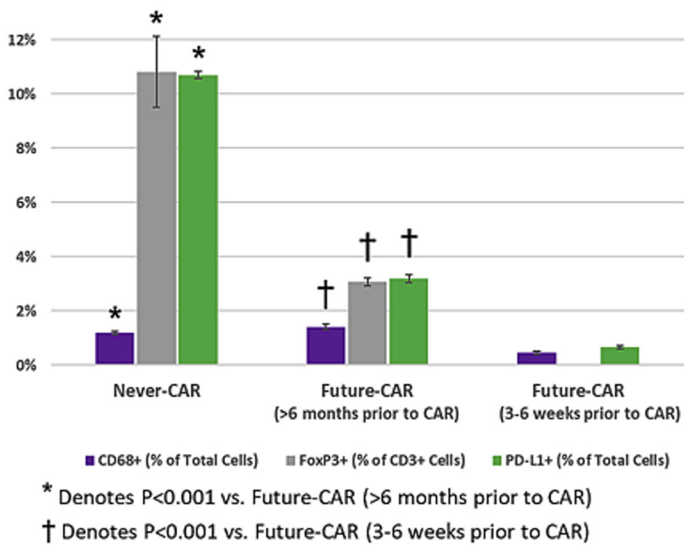

QmIF results for CD68+, FoxP3+, and PD-L1+ cells, grouped by future CAR risk and temporal proximity to a high-grade, clinically evident rejection event. Never-CAR cases have markedly higher proportions of immune-modulating FoxP3 and PD-L1 than do future-CAR cases. Future-CAR cases when assessed by temporal proximity to a serious rejection event demonstrate an almost complete loss of detectable IF signal for each of these potentially allograft-protective markers by 3 to 6 weeks prior to serious rejection. **Error bars** = SE. $p < 0.001$ versus future CAR at *>6 months or †3 to 6 weeks prior to CAR. Abbreviations as in Figures 1 and 2.

consideration of more than just a rough count of basophilic immune cells as performed in conventional ISHLT grading is required. This hypothesis is reinforced when the concordant low ISHLT grade EMB are differentiated from one another as future-rejection cases versus never-rejection cases, based on whether the patient experiences a serious rejection event in the first 3 years post-transplantation. The immune profiles of never-rejection EMB are defined by particularly high proportions of PD-L1+ and FoxP3+ cells. In contrast, future-rejection EMB as a whole exhibit lower levels of these allo-protective markers, with striking reductions observed by 3 to 6 weeks prior to an upcoming clinically evident rejection. The nearly complete loss of FoxP3+ and PD-L1+ cells in the weeks preceding clinically evident rejection supports both their potential utility as biomarkers for identifying patients at high risk for significant rejection events, as well as the need to further investigate potential allo-protective role of these markers in heart transplantation.

Mechanistically, the interplay between monocyte lineage cells (CD68+), regulatory T cells (FoxP3+), and PD-L1-expressing cells suggested by our results has been the focus of significant biomedical research, though rarely in the context of organ transplantation (40–47). The binding of PD-L1 to PD1 on helper T cells, beyond simple "inactivation" with consequent decreases in inflammatory cytokine production, has been shown to stimulate FoxP3+ expression and effector T-cell differentiation into regulatory T cells (41,42,44,45). Macrophages and regulatory T cells can interact in a synergistic fashion, with cytokines produced by regulatory T cells encouraging macrophages to differentiate into M2 anti-inflammatory macrophages. In turn, M2 macrophages secrete specific cytokines and express PD-L1, both of which can facilitate further helper T-cell differentiation into regulatory T cells. These established mechanisms lend immunologic plausibility to our findings, though confirmation of these mechanisms within allograft tissues is beyond the scope of the present work.

STUDY LIMITATIONS. The results we have presented must be considered in the context of the limited sample size both in terms of patients and EMB events, and generalizing these findings should be done with caution. Nevertheless, the high numbers of cells analyzed along with the unbiased computational methods used to analyze them provide reassurance that the phenomena uncovered in this cohort are valid within this cohort. We also recognize that the discordant high ISHLT grade designation is an area of some uncertainty, because it is standard practice for all high ISHLT grade biopsy events to receive some form of altered immunosuppression regardless of the presence (or absence) of abnormal clinical diagnostic data. Thus, a more serious clinical trajectory could potentially have been averted by early alterations in therapy in these false-positive cases, with no way to know for certain whether the rejection event was destined to remain clinically silent. However, these discordant high ISHLT grade cases met none of the clinical criteria for clinically evident rejection, and our study findings seem to support the existence of different immunobiologies in comparison to concordant high ISHLT grade cases. It is also worth noting that prior case series demonstrating benign clinical courses with certain untreated high ISHLT grade EMB support the theory that there are distinct phenotypes with distinct fates existing within the traditional high ISHLT grade grouping (1). Finally, the relatively high rate of technical failure of the QmIF analysis (26% of EMB) is a concern, but it may reflect our dependence on residual material following routine clinical processing and the 6- to 12-year interval between EMB sampling and QmIF analysis in this experiment.

FUTURE DIRECTIONS. Considering future opportunities, it should be noted that the present QmIF

panel was far from exhaustive with regard to exploring all of the relevant immune cell populations/effectors that may have diagnostic or prognostic value for CAR. Certainly, future research can apply additional QmIF antibody panels to further explore mechanisms of interest. Additionally, the present research does not fully leverage the available tools for quantitative image analysis in modern digital pathology. Spatial relationships between markers and infiltration patterns can be quantified using modern computer algorithms (48,49) and may provide additional layers of detail that enhance our understanding of disease while also boosting diagnostic and predictive performance. Finally, the present work may be enhanced by integrating complementary molecular technologies to better characterize the allograft-specific antigen targets of T-cell immunity that may play a role in determining CAR severity and future risk. The checkpoint inhibitor therapies and engineered cell therapies that have revolutionized oncologic medicine are based on 2 fundamental immunologic concepts: that cells have the ability to evade T-cell immune responses utilizing inhibitory surface receptors (e.g., PD-L1), and that a detailed molecular understanding of antigen immunogenicity can permit robust in vivo targeting of specific tissues via engineered T cells. Whereas our present work closely resembles the early in situ research that elucidated the role of checkpoint molecules in tumor tissues (50), future efforts should also focus on characterizing which allograft antigens play a role in determining the allograft fate via T-cell receptor sequencing.

CONCLUSIONS

Although there is indeed important additional work to be performed, the present research represents an important step toward precision diagnosis and risk stratification in cardiac transplantation. Our results demonstrate the feasibility and translational potential of the QmIF methodology, while identifying several key, and potentially targetable, mechanisms involved in determining the severity of an alloimmune response.

ADDRESS FOR CORRESPONDENCE: Dr. Kenneth B. Margulies, Perelman School of Medicine, University of Pennsylvania, Translational Research Center, Room 11-101, 3400 Civic Center Boulevard, Building 421, Philadelphia, Pennsylvania 19104. E-mail: ken.margulies@uphs.upenn.edu.

PERSPECTIVES

COMPETENCY IN MEDICAL KNOWLEDGE: Clinically, these proof-of-concept studies support the feasibility and clinical benefits of applying immune-phenotyping for characterization of cardiac allograft biopsies. Specifically, the findings that the abundance of regulatory T cells and PD-L1 expression is linked to clinical allograft status suggests that native rejection suppressing processes may contribute to the discordance frequently observed between patients' clinical trajectory and ISHLT biopsy grade. The findings that suppressed PD-L1 is linked to clinically significant allo-immunity is a relevant extension of recent reports that checkpoint molecule inhibitors can induce severe myocarditis.

TRANSLATIONAL OUTLOOK: From a translational perspective, the implicated allo-protective actions of CD68-expressing macrophages, FoxP3-expressing regulatory T cells, and PD-L1 expression merit both further mechanistic investigation in preclinical animal models and clinical investigation in larger retrospective and prospective cohorts, including a greater emphasis on time-course studies. Enhanced mechanistic clarity will ultimately enable more precise immune-suppressive strategies with superior performance for recipients of solid organ transplants.

REFERENCES

1. Klingenberg R, Koch A, Schnabel PA, et al. Allograft rejection of ISHLT grade >/=3A occurring late after heart transplantation—a distinct entity? J Heart Lung Transplant 2003;22:1005–13.

2. Kobashigawa JA. The search for a gold standard to detect rejection in heart transplant patients: are we there yet? Circulation 2017;135:936–8.

3. Pham MX, Teuteberg JJ, Kfoury AG, et al., for the IMAGE Study Group. Gene-expression profiling for rejection surveillance after cardiac transplantation. N Engl J Med 2010;362:1890–900.

4. Dandel M, Hummel M, Meyer R, et al. Left ventricular dysfunction during cardiac allograft rejection: early diagnosis, relationship to the histological severity grade, and therapeutic implications. Transplant Proc 2002;34:2169–73.

5. Stewart S, Winters GL, Fishbein MC, et al. Revision of the 1990 working formulation for the standardization of nomenclature in the diagnosis of heart rejection. J Heart Lung Transplant 2005;24:1710–20.

6. Wang C, Gong J, Tu TY, Lee PP, Fakih M. Immune profiling of microsatellite instability-high and polymerase ε (*POLE*)-mutated metastatic colorectal tumors identifies predictors of response to anti-PD-1 therapy. J Gastrointest Oncol 2018;9:404–15.

7. van den Berg TK, Valerius T. Myeloid immune-checkpoint inhibition enters the clinical stage. Nat Rev Clin Oncol 2019;16:275–6.

8. Galon J, Bruni D. Approaches to treat immune hot, altered and cold tumours with combination immunotherapies. Nat Rev Drug Discov 2019;18:197–218.

9. Wang YL, Gao JM, Xing LZ. Therapeutic potential of Oroxylin A in rheumatoid arthritis. Int Immunopharmacol 2016;40:294–9.

10. Wehr P, Purvis H, Law SC, Thomas R. Dendritic cells, T cells and their interaction in rheumatoid arthritis. Clin Exp Immunol 2019;196:12–27.

11. Kim N, Kim HS. Targeting checkpoint receptors and molecules for therapeutic modulation of natural killer cells. Front Immunol 2018;9:2041.

12. Burugu S, Dancsok AR, Nielsen TO. Emerging targets in cancer immunotherapy. Semin Cancer Biol 2018;52:39–52.

13. Stack EC, Wang C, Roman KA, Hoyt CC. Multiplexed immunohistochemistry, imaging, and quantitation: a review, with an assessment of Tyramide signal amplification, multispectral imaging and multiplex analysis. Methods 2014;70:46–58.

14. Parra ER, Uraoka N, Jiang M, et al. Validation of multiplex immunofluorescence panels using multispectral microscopy for immune-profiling of formalin-fixed and paraffin-embedded human tumor tissues. Sci Rep 2017;7:13380.

15. Blom S, Paavolainen L, Bychkov D, et al. Systems pathology by multiplexed immunohistochemistry and whole-slide digital image analysis. Sci Rep 2017;7:15580.

16. Galetta H, Mansfield J, Richard B, et al. Validation of multiplex immunofluorescence for use in analysis of tumour infiltrating lymphocytes. J Immunotherapy Cancer 2015;3:P411.

17. Gorris MAJ, Halilovic A, Rabold K, et al. Eight-color multiplex immunohistochemistry for simultaneous detection of multiple immune checkpoint molecules within the tumor microenvironment. J Immunol 2018;200:347–54.

18. Harper SJ, Ali JM, Wlodek E, et al. CD8 T-cell recognition of acquired alloantigen promotes acute allograft rejection. Proc Natl Acad Sci U S A 2015;112:12788–93.

19. Rocha PN, Plumb TJ, Crowley SD, Coffman TM. Effector mechanisms in transplant rejection. Immunol Rev 2003;196:51–64.

20. Le Moine A, Goldman M, Abramowicz D. Multiple pathways to allograft rejection. Transplantation 2002;73:1373–81.

21. Bestard O, Cruzado JM, Rama I, et al. Presence of FoxP3+ regulatory T cells predicts outcome of subclinical rejection of renal allografts. J Am Soc Nephrol 2008;19:2020–6.

22. Chung BH, Oh HJ, Piao SG, et al. Clinical significance of the ratio between FOXP3 positive regulatory T cell and interleukin-17 secreting cell in renal allograft biopsies with acute T-cell-mediated rejection. Immunology 2012;136:344–51.

23. Hua J, Inomata T, Chen Y, et al. Pathological conversion of regulatory T cells is associated with loss of allotolerance. Sci Rep 2018;8:7059.

24. Raimondi G, Sumpter TL, Matta BM, et al. Mammalian target of rapamycin inhibition and alloantigen-specific regulatory T cells synergize to promote long-term graft survival in immunocompetent recipients. J Immunol 2010;184:624–36.

25. Liao T, Xue Y, Zhao D, et al. In vivo attenuation of antibody-mediated acute renal allograft rejection by ex vivo TGF-β-induced CD4(+)Foxp3(+) regulatory T cells. Front Immunol 2017;8:1334.

26. Tinckam KJ, Djurdjev O, Magil AB. Glomerular monocytes predict worse outcomes after acute renal allograft rejection independent of C4d status. Kidney Int 2005;68:1866–74.

27. Girlanda R, Kleiner DE, Duan Z, et al. Monocyte infiltration and kidney allograft dysfunction during acute rejection. Am J Transplant 2008;8:600–7.

28. Alhamad T, Venkatachalam K, Linette GP, Brennan DC. Checkpoint inhibitors in kidney transplant recipients and the potential risk of rejection. Am J Transplant 2016;16:1332–3.

29. Goldman JW, Abdalla B, Mendenhall MA, et al. PD 1 checkpoint inhibition in solid organ transplants: 2 sides of a coin—case report. BMC Nephrol 2018;19:210.

30. Lipson EJ, Bagnasco SM, Moore J Jr., et al. Tumor regression and allograft rejection after administration of anti-PD-1. N Engl J Med 2016;374:896–8.

31. Pilat N, Sayegh MH, Wekerle T. Costimulatory pathways in transplantation. Semin Immunol 2011;23:293–303.

32. Tanaka K, Albin MJ, Yuan X, et al. PDL1 is required for peripheral transplantation tolerance and protection from chronic allograft rejection. J Immunol 2007;179:5204–10.

33. Schütte-Nütgen K, Boenisch O, Harrach H, et al. Divergent function of programmed death-ligand 1 in donor tissue versus recipient immune system in a murine model of bronchiolitis obliterans. Am J Pathol 2017;187:1368–79.

34. Costanzo MR, Dipchand A, Starling R, et al. The International Society of Heart and Lung Transplantation Guidelines for the care of heart transplant recipients. J Heart Lung Transplant 2010;29:914–56.

35. Kobashigawa JA, Miller LW, Russell SD, et al. Tacrolimus with mycophenolate mofetil (MMF) or sirolimus vs. cyclosporine with MMF in cardiac transplant patients: 1-year report. Am J Transplant 2006;6:1377–86.

36. Eisen HJ, Tuzcu EM, Dorent R, et al., for the RAD B253 Study Group. Everolimus for the prevention of allograft rejection and vasculopathy in cardiac-transplant recipients. N Engl J Med 2003;349:847–58.

37. Kobashigawa J, Patel J, Azarbal B, et al. Randomized pilot trial of gene expression profiling versus heart biopsy in the first year after heart transplant: early invasive monitoring attenuation through gene expression trial. Circ Heart Fail 2015;8:557–64.

38. Igarashi T, Teramoto K, Ishida M, Hanaoka J, Daigo Y. Scoring of PD-L1 expression intensity on pulmonary adenocarcinomas and the correlations with clinicopathological factors. ESMO Open 2016;1:e000083.

39. Berry GJ, Burke MM, Andersen C, et al. The 2013 International Society for Heart and Lung Transplantation Working Formulation for the standardization of nomenclature in the pathologic diagnosis of antibody-mediated rejection in heart transplantation. J Heart Lung Transplant 2013;32:1147–62.

40. Schmidt A, Zhang XM, Joshi RN, et al. Human macrophages induce CD4(+)Foxp3(+) regulatory T cells via binding and re-release of TGF-beta. Immunol Cell Biol 2016;94:747–62.

41. Amarnath S, Magnus CW, Wang JC, et al. The PDL1-PD1 axis converts human TH1 cells into regulatory T cells. Sci Transl Med 2011;3:111ra120.

42. Francisco LM, Salinas VH, Brown KE, et al. PD-L1 regulates the development, maintenance, and function of induced regulatory T cells. J Exp Med 2009;206:3015–29.

43. Romano M, Fanelli G, Tan N, et al. Expanded regulatory T cells induce alternatively activated monocytes with a reduced capacity to expand T helper-17 cells. Front Immunol 2018;9:1625.

44. Gianchecchi E, Fierabracci A. Inhibitory receptors and pathways of lymphocytes: the role of PD-1 in Treg development and their involvement in autoimmunity onset and cancer progression. Front Immunol 2018;9:2374.

45. Miao X, Xu R, Fan B, et al. PD-L1 reverses depigmentation in Pmel-1 vitiligo mice by increasing the abundance of Tregs in the skin. Sci Rep 2018;8:1605.

46. Zhao Y, Chen S, Lan P, et al. Macrophage subpopulations and their impact on chronic allograft rejection versus graft acceptance in a mouse heart transplant model. Am J Transplant 2018;18:604–16.

47. Grabie N, Lichtman AH, Padera R. T cell checkpoint regulators in the heart. Cardiovasc Res 2019;115:869–77.

48. Nirschl JJ, Janowczyk A, Peyster EG, et al. A deep-learning classifier identifies patients with clinical heart failure using whole-slide images of H&E tissue. PLoS One 2018;13:e0192726.

49. Peyster EG, Madabhushi A, Margulies KB. Advanced morphologic analysis for diagnosing allograft rejection: the case of cardiac transplant rejection. Transplantation 2018;102:1230–9.

50. Hutloff A, Dittrich AM, Beier KC, et al. ICOS is an inducible T-cell co-stimulator structurally and functionally related to CD28. Nature 1999;397:263–6.

KEY WORDS allograft rejection, immune checkpoint molecules, immune regulation, quantitative immunohistochemistry

APPENDIX For supplemental tables, please see the online version of this paper.

Go to http://www.acc.org/jacc-journals-cme to take the CME/MOC/ECME quiz for this article.